PAPER

A three dimensional vertically aligned multiwall carbon nanotube/NiCo₂O₄ core/shell structure for novel high-performance supercapacitors†

Wen-wen Liu,‡[a] Congxiang Lu,‡[ab] Kun Liang[a] and Beng Kang Tay*[ab]

Three dimensional (3D) vertically aligned structures have attracted tremendous attention from scientists in many fields due to their unique properties. In this work, we have built the 3D vertically aligned carbon nanotube (CNT)/NiCo₂O₄ core/shell nanoarchitecture *via* a facile electrochemical deposition method followed by subsequent annealing in air. The morphology and structure have been in-depth characterized by SEM, TEM, XRD and Raman spectroscopy. Impressively, when used as the electrode material in a 6 M KOH electrolyte, the vertically aligned CNT/NiCo₂O₄ core/shell structures exhibit excellent supercapacitive performances, including high specific capacitance, excellent rate capability and good cycle stability. This is due to the unique 3D vertically aligned CNT/NiCo₂O₄ core/shell structures, which support high electron conductivity, large surface area of NiCo₂O₄ and fast ion/electron transport in the electrode and at the electrolyte–electrode interface. Furthermore, the synthesis strategy presented here can be easily extended to fabricate other metal oxides with a controlled core/shell structure, which may be a promising facile strategy for high performance supercapacitors, and even advanced Li-ion batteries.

1. Introduction

Because of the limited availability of fossil fuels and the increasingly urgent concerns about the environmental impact of conventional energy technologies, supercapacitors, also known as electrochemical capacitors, have attracted great attention as "green" and renewable energy storage devices due to their excellent performances, including ultra-high power density, long cycling stability, wide operation temperature range and improved safety.[1–7] However, compared with batteries and fuel cells, supercapacitors have relatively lower energy density,[8] which has restricted their potential applications to certain extent. Therefore, improvement of supercapacitors is crucial to meet the future energy demands. An efficient way is to seek for the novel materials with good capacitive characteristics such as both high energy and power densities.

To date, various materials, including carbonaceous materials, transition metal oxides (TMOs), conductive polymers, and hybrid composites, have been widely studied as electrodes for supercapacitors.[9–11] Among them, TMOs, such as Fe₃O₄,[12]

Co₃O₄,[13–15] NiO,[16,17] ZnO,[18] SnO₂,[19] V₂O₅,[20,21] and MnO₂[22,23] have attracted intense attention due to their multiple oxidation states/structures that enable rich redox reactions, high specific capacitance, low cost and environmental friendliness. However, because of the intrinsic poor electrical conductivity and the short diffusion distance of electrolytes,[24] only the surface part of these active materials can effectively contribute to the total capacitance while the underneath part could hardly participate in the electrochemical charge storage process, leading to a less satisfactory performance.[24,25] Therefore, it is still a great challenge to boost the electrochemical utilization and the specific capacitance of TMOs.

Recently, spinel nickel cobaltite (NiCo₂O₄) has been proved to be a very promising electrode material since it offers many intriguing advantages such as low-cost, abundant resources and environmental friendliness.[26–28] More significantly, NiCo₂O₄ possesses a much better electrical conductivity, at least two orders of magnitude higher, and higher electrochemical activity than nickel oxides and cobalt oxides.[26,29] These attractive features are beneficial to the development of high-performance supercapacitors. It is interesting to note that many efforts have been made to improve the supercapacitive performance of NiCo₂O₄ through the different methods of adjusting the morphology (nanorods, nanowires, nanoplates and nanoneedles),[30–33] pore size (micropores and mesoporous)[34–36] and so forth. However, there are still many challenges for NiCo₂O₄-based electrode materials to meet the new and high requirements for future applications. Fortunately, it is reported that

[a] Novitas, Nanoelectronics Center of Excellence, School of Electrical and Electronic Engineering, Nanyang Technological University, Singapore 639798. E-mail: ebktay@ntu.edu.sg; Tel: +65 67906783

[b] CINTRA CNRS/NTU/THALES, Nanyang Technological University, Singapore 637553

† Electronic supplementary information (ESI) available. See DOI: 10.1039/c4ta00107a

‡ These two authors contributed equally to this work.

the rational design of electrode materials with well-defined micro-/nanostructures is imperative for the further enhancement of the electrochemical properties by improving the kinetics of ion diffusion and electronic conductivity.[2,26,37] To the best of our knowledge, there are few reports on the rational design of a homogeneous core/shell $NiCo_2O_4$ array for supercapacitors, though the capacitive property of $NiCo_2O_4$ has been extensively investigated.

In this work, on the basis of the above considerations, we have built a three dimensional (3D) vertically aligned CNT/$NiCo_2O_4$ core/shell nanoarchitecture electrode *via* a facile electrochemical deposition method followed by subsequent annealing in air. In this electrode design, vertically aligned highly conductive CNTs are used as the "cores" to support the $NiCo_2O_4$, enhancing its rate capability by shortening the distance for electron transport. Moreover, compared with the common coating electrode used for electrochemical measurement, the 3D vertically aligned CNT/$NiCo_2O_4$ core/shell structure electrode is binder-free, which can provide more active sites for the active material to come in contact with the electrolyte. We have further investigated the properties of the 3D vertically aligned CNT/$NiCo_2O_4$ core/shell structure electrode for supercapacitors, which exhibits excellent electrochemical characteristics in 6 M KOH solution. Because of the advantages of this structure, such as fast ion and electron transfer, large number of active sites and good strain accommodation, the 3D vertically aligned CNT/$NiCo_2O_4$ core/shell structure electrode may have potential applications in supercapacitors and other energy storage devices.

2. Experimental

2.1 Growth of vertically aligned CNTs on stainless steel

After sequential ultrasonic cleaning in acetone, isopropyl alcohol and de-ionized water, the round stainless steel (SS) foil with diameters of 1.5 cm were blow-dried by N_2 and baked in an oven. The SS foil was then coated with a TiN barrier layer in an Elite sputtering system, followed by electron beam deposition of the thin Ni layer as a catalyst in an Auto 306, HHV system. Vertically aligned CNT growth was carried out in a Nano Instrument plasma enhanced chemical vapor deposition (PECVD) system at 800 °C for 10 min in the atmosphere of 240 sccm NH_3 and 60 sccm C_2H_2 at the pressure of 9.0 mbar. A radio frequency (RF) electric field was applied and biased at 700 V in the chamber with a power of 120 W.

2.2 Preparation of the 3D vertically aligned CNT/$NiCo_2O_4$ core/shell structure electrode

All the chemicals were of analytical grade and used without further purification. The obtained SS supported vertically aligned CNTs were firstly treated by O_2 plasma at a RF power of 30 W for 10 seconds to change the wettability before the electrochemical deposition (see ESI Fig. S1†). Also, the backside of the SS was protected by polytetrafluoroethylene (PTFE) tapes to prevent formation of $NiCo_2O_4$ there. The co-electrodeposition was performed in a standard three-electrode system with the

SS substrate-supported vertically aligned CNTs as the working electrode, a platinum plate as the counter electrode and a saturated calomel electrode (SCE) as the reference electrode at room temperature. The electrodeposition of the bimetallic (Ni, Co) hydroxide precursor upon the CNT array was carried out at −1.0 V (*vs.* SCE) in a 4 mM $Co(NO_3)_2 \cdot 6H_2O$ and 2 mM $Ni(NO_3)_2 \cdot 6H_2O$ mixed electrolyte using a Solartron (1287 + 1260) electrochemical workstation. After electrodeposition for 10 min, the sample with green surface was carefully rinsed several times with de-ionized water, and finally dried at 60 °C in air. Subsequently, the sample was put in a quartz tube and calcined at 300 °C for 2 h with a ramping rate of 1 °C min^{-1} to transform the precursor into ultrathin porous $NiCo_2O_4$ nanosheets. On average, the mass of $NiCo_2O_4$ nanosheets grown on the CNT array is 0.62 mg, which was obtained by carefully measuring the samples before electrodeposition and after thermal annealing using a high precision electronic balance.

2.3 Material characterization and electrochemical measurements

A field emission scanning electron microscope (FESEM, LEO 1550 GEMINI) was employed to study the morphology of the as-prepared samples. Transmission electron microscopy (TEM), high resolution TEM (HRTEM), scanning TEM (STEM) and energy-dispersive X-ray spectroscopy (EDX) mapping were carried out using a JEOL JEM 2100 F. X-ray diffraction (XRD) patterns were collected on powder XRD (Max 18 XCE, Japan) using a Cu Kα source ($\lambda = 0.154056$ nm). Raman spectra were obtained using a WITec CRM200 Raman system and the 532 nm line of an argon ion laser was used as the excitation source in all the measurements.

All electrochemical measurements were carried out using a Solartron (1287 + 1260) electrochemical workstation in an open three-electrode cell system at room temperature. A slice of platinum and a SCE were used as the auxiliary electrode and the reference electrode, respectively. The cyclic voltammetry (CV) tests were measured with the potential window from 0 to 0.5 V (*vs.* SCE) at different scan rates varying from 5 to 100 mV s^{-1}. The electrochemical impedance spectroscopy (EIS) plots were tested in the frequency ranging from 100 kHz to 0.05 Hz at open circuit potential with an AC perturbation of 5 mV. Galvanostatic charge/discharge tests were measured with the constant current density ranging from 1 to 10 A g^{-1}. The experiments were performed at room temperature in 6.0 M KOH electrolyte solution. The specific capacitance was calculated from the discharge curves by the formula:

$$C = \frac{I\Delta t}{m\Delta V} \tag{1}$$

The specific energy density and power density are defined respectively by:

$$E = \frac{C\Delta V^2}{7.2} \tag{2}$$

This journal is © The Royal Society of Chemistry 2014

J. Mater. Chem. A, 2014, **2**, 5100–5107 | **5101**

and

$$P = \frac{E \times 3600}{t} \qquad (3)$$

here, C is the specific capacitance (F g^{-1}), I is the constant discharging current (A g^{-1}), Δt in s is the discharge time (s), ΔV is the potential window during the discharge process after internal resistance (IR) drop (V), m is the total mass of the two electrode materials (g), E is the energy density (W h kg^{-1}) and P is the power density (W kg^{-1}).

3. Results and discussion

The co-electrodeposition preparation of spinel NiCo$_2$O$_4$ on the SS substrate-supported vertically aligned CNTs mainly includes a co-electrodeposition step and a post-annealing treatment step. Firstly, the mixed (Ni, Co) hydroxide precursor is co-electrodeposited onto the treated CNT array *via* a three-electrode system, where the SS substrate-supported vertically aligned CNTs, a slice of platinum and a saturated calomel electrode (SCE) are used as the working, auxiliary and reference electrodes (Fig. 1a), respectively. In this electrodeposition process, NO$_3^-$ is reduced on the cathodic surface accompanied by the production of OH$^-$ ions. Then, the generation of OH$^-$ ions raises the pH value in the vicinity of the working electrode, resulting in the uniform precipitation of mixed (Ni, Co) hydroxide on the surface of CNTs. This process may comprise the electrochemical reactions and subsequent precipitation of mixed hydroxide, as described by the following three equations:[38–40]

$$NO_3^- + H_2O + 2e^- \rightarrow NO_2^- + 2OH^- \qquad (4)$$

$$NO_2^- + 6H_2O + 6e^- \rightarrow NH_4^+ + 8OH^- \qquad (5)$$

$$xNi^{2+} + 2xCo^{2+} + 6xOH^- \rightarrow Ni_xCo_{2x}(OH)_{6x} \qquad (6)$$

Secondly, the green bimetallic (Ni, Co) hydroxide precursor is converted into black spinel NiCo$_2$O$_4$ supported on the CNT array by a simple annealing treatment in air (Fig. 1b and c) as follows:[38]

$$Ni_xCo_{2x}(OH)_{6x} + 1/2xO_2 \rightarrow xNiCo_2O_4 + 3xH_2O \qquad (7)$$

The phase, crystallinity, and purity of the as-prepared samples are determined by X-ray diffraction (XRD) measurements. Herein, for XRD analysis, the vertically aligned CNT/NiCo$_2$O$_4$ core/shell structures are scratched from the SS substrate in order to preclude the strong impact of the SS substrate (see ESI Fig. S2†). As shown in Fig. 2a, the diffraction peaks are well indexed as the spinel NiCo$_2$O$_4$ crystalline structure (JCPDS: 20-0781) and no excrescent peaks from other crystallized phases are detected, implying the formation of the pure spinel NiCo$_2$O$_4$ structure obtained by the electrodeposition and thermal treatment.[39–41] However, the relative broad patterns demonstrate that the NiCo$_2$O$_4$ crystals have small sizes or relative low crystallinity. Moreover, no sharp peaks of CNTs are detected, suggesting that the CNTs are homogeneously surrounded by NiCo$_2$O$_4$. Fig. 2b shows that NiCo$_2$O$_4$ adopts the spinel structure (space group $Fd3m$) with Ni atoms located in the octahedral sites and Co atoms occupying both octahedral and tetrahedral sites, which provides a 3D network of tunnels for ion diffusion. Furthermore, Raman spectroscopy is also used to characterize the phase composition of the CNT/NiCo$_2$O$_4$ core/shell array structure. As seen in ESI Fig. S3,† the peaks at 213, 470, 551, and 676 cm^{-1} correspond to F$_{2g}$, E$_g$, F$_{2g}$, and A$_{1g}$ modes of the NiCo$_2$O$_4$, respectively.[2] In addition, two peaks at 1307 cm^{-1} and 1614 cm^{-1} were observed, attributed to the D band and the G band of the CNT array.[42]

Field emission scanning electron microscopy (FESEM) is used to study the surface morphology of the prepared 3D vertically aligned CNT/NiCo$_2$O$_4$ core/shell structures. As shown in Fig. 3a, the CNTs grown on the SS substrate are homogeneously aligned and separated apart adequately, forming a unique nanoarray. Moreover, as can be seen from the inset of Fig. 3a, the surface of the CNTs is smooth and the diameter of CNTs is around 80–150 nm. After the electrodeposition and annealing process, the surface of the CNT array is fully covered by the NiCo$_2$O$_4$ layer (Fig. 3b and c), forming a vertically aligned CNT/NiCo$_2$O$_4$ core/shell structure. In addition, the high-magnification image (Fig. 3d) illustrates that the NiCo$_2$O$_4$ nanosheets are ultrathin, which are highly accessible for the electrolyte and beneficial for the full utilization when used as an electrode material for supercapacitors.

To gain further insight into the morphology and microstructure of the as-prepared 3D vertically aligned CNT/NiCo$_2$O$_4$ core/shell structure, TEM, HRTEM and energy-dispersive X-ray spectroscopy (EDX) are performed. Compared with the TEM image of pure CNTs (see ESI Fig. S4†), it is evidently observed that the highly conductive CNT "core" is tightly bonded and totally covered with ultrathin NiCo$_2$O$_4$ nanosheets (Fig. 4a), forming a typical core/shell heterostructured architecture, which is consistent with the above FESEM observation. Especially, there is no clear interface observed from the TEM image
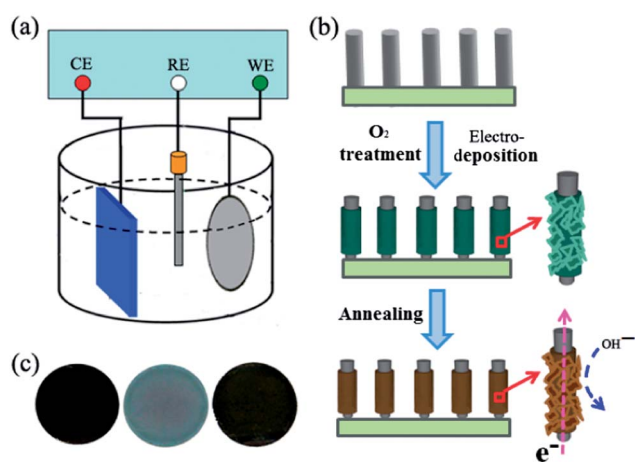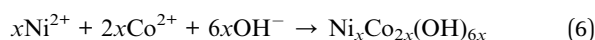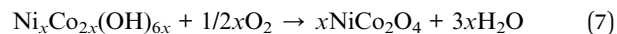

Fig. 1 (a) Schematic of the apparatus for electrochemical deposition of the bimetallic (Ni, Co) hydroxide precursor on the SS substrate-supported vertically aligned CNTs, (b) schematic illustration of the formation process of the vertically aligned CNT/NiCo$_2$O$_4$ core/shell structure, and (c) digital photos of SS substrate-supported bare vertically aligned CNTs after depositing the bimetallic (Ni, Co) hydroxide precursor followed by the annealing in air (left to right), respectively.

5102 | J. Mater. Chem. A, 2014, 2, 5100–5107

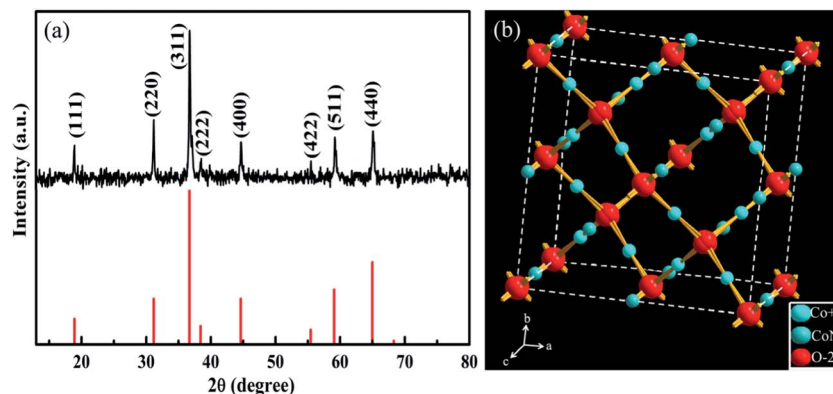This journal is © The Royal Society of Chemistry 2014

Fig. 2 (a) XRD pattern and (b) crystal structure of the as-synthesized $NiCo_2O_4$.
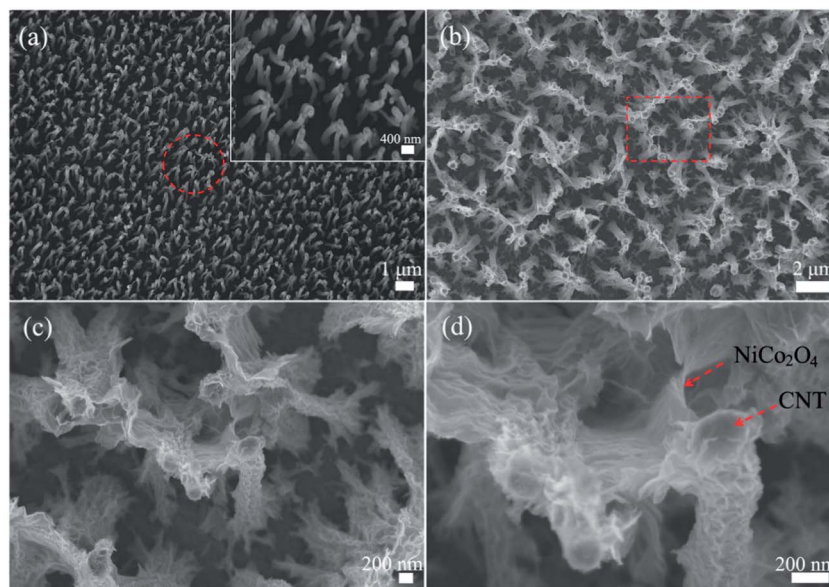

Fig. 3 (a) FESEM images of bare 3D CNT array, (b–d) FESEM images with different magnifications for the 3D vertically aligned CNT/$NiCo_2O_4$ core/shell structure. The inset in panel (a) is an enlargement of the part indicated by the circle in panel (a). The image in (c) is taken from the region marked with the rectangle in panel (b).

between the CNT "core" and the $NiCo_2O_4$ "shell", suggesting the penetrative growth of $NiCo_2O_4$ nanosheets onto the CNT array. From the relatively higher magnification TEM image (Fig. 4b), it can be seen that the thickness of the outer symmetric $NiCo_2O_4$ "shell" layer is about 27 nm. Also, it reveals that the as-prepared $NiCo_2O_4$ samples are typically nanosheets with small and dense nanopores, which result from the thermal decomposition of the Ni, Co-hydroxide precursor nanosheets.[4] What is more, these small and dense nanopores are advantageous for the ions in and out during the charge/discharge process. The high resolution TEM (HRTEM) examination (Fig. 4c) clearly shows that the lattice phase has random orientation, demonstrating the polycrystalline nature of the as-prepared $NiCo_2O_4$ sample. Additionally, the space between adjacent fringes are 0.48 nm and 0.27 nm, which correspond to the (111) and (220) lattice spaces of spinel $NiCo_2O_4$, respectively, which agree well with previous reports.[39–41] Besides, the EDX spectroscopy (Fig. 4d), conducted

in the blue circle area of Fig. 4b, shows that Ni and Co elements are detected, and the atomic proportion of Ni to Co is close to 1 : 2, in agreement with the stoichiometric ratio of $NiCo_2O_4$. According to the aforementioned morphology and microstructure characterizations of SEM, TEM, XRD and Raman spectroscopy, the vertically aligned CNT/$NiCo_2O_4$ core/shell structures have been successfully prepared *via* a facile electrodeposition method followed by the annealing treatment in air.

Cyclic voltammetry (CV), galvanostatic charge/discharge and electrochemical impedance response measurements (EIS) are employed to investigate the electrochemical properties of the obtained vertically aligned CNT/$NiCo_2O_4$ core/shell structure as the electrode for supercapacitors. CV tests (Fig. 5a) are characterized in a three-electrode system with 6 M KOH solution as the electrolyte at the various scan rates in the potential range from 0 to 0.5 V. Clearly, there are two anodic peaks at 0.32 and 0.41 V (corresponding to cathodic peaks at 0.28 V and 0.37 V) observed
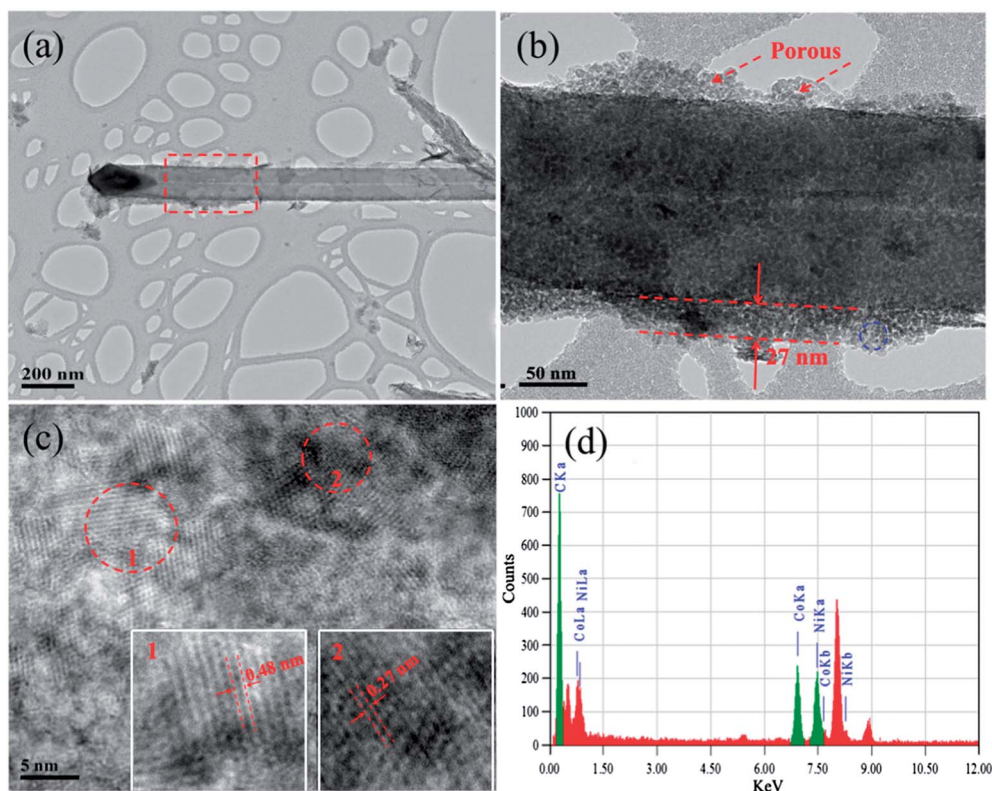
This journal is © The Royal Society of Chemistry 2014

J. Mater. Chem. A, 2014, 2, 5100–5107 | 5103

Fig. 4 (a and b) TEM and (c) HRTEM images, and (d) EDX of the 3D vertically aligned CNT/NiCo$_2$O$_4$ core/shell structure. The image (b) is taken from the region marked with the rectangle in panel (a). The inset images 1 and 2 in panel (c) are the enlargements of 1 and 2 indicated by the circles in panel (c), respectively.

from the CV curve of the 3D CNT/NiCo$_2$O$_4$ nanosheets core/shell array electrode at the 5 mV s^{-1}, indicating that the capacitive characteristics are mainly governed by the Faradaic reaction. Herein, the two redox peaks can be attributed to the redox reactions of Ni and Co species in the alkaline electrolyte based on the following equations:[34,43]

$$NiCo_2O_4 + OH^- + H_2O \leftrightarrow NiOOH + 2CoOOH + 2e^- \quad (8)$$

Surprisingly, with 20-fold increase in the scan rate from 5 to 100 mV s^{-1}, the anodic/cathodic peak shifts toward the positive/ negative potential respectively, and the redox current increases. This observation reveals the low resistance of the electrode and the super-fast electronic transport rate between the vertically aligned CNT/NiCo$_2$O$_4$ core/shell structure and the conductive SS substrate, which can be further proved by EIS (see ESI Fig. S5†). Besides, it can be seen that the SS substrate-supported bare vertically aligned CNT electrode has a very small area surrounded by the CV curve compared with that of the vertically aligned CNT/NiCo$_2$O$_4$ core/shell structure electrode at the same scan rate, suggesting that the capacitance contribution from the substrate and CNTs is negligible (see ESI Fig. S6†).

To further calculate the specific capacitance and also understand the rate capability of the vertically aligned CNT/ NiCo$_2$O$_4$ core/shell structure electrode, the charge/discharge measurements are performed with the potential window

between 0 and 0.41 V at different current densities (Fig. 5b). As can be seen from the constant current charge/discharge curves, the shapes of these curves are very similar and show ideal capacitive behavior with very sharp responses and small internal resistance (IR) drops. In addition, it can be clearly observed that the voltage plateaus appearing in the charge/ discharge curves match well with the peaks observed in the CV curves (Fig. 5b), which further reveals the typical pseudo-capacitance behavior of the vertically aligned CNT/NiCo$_2$O$_4$ core/shell structure electrode. The specific capacitances (Fig. 5c), calculated from the discharge time according to eqn (1), are 695, 656, 638, 591, and 576 F g^{-1} corresponding to the discharge current densities of 1, 2, 4, 10, and 20 A g^{-1}, respectively. The specific capacitance gradually decreases with the increase of the current densities from 1 to 20 A g^{-1}, but the as-fabricated vertically aligned CNT/NiCo$_2$O$_4$ core/shell structure electrode still remains nearly 82% of the initial capacitance value even at a high current density of 20 A g^{-1}, which manifests that the vertically aligned CNT/NiCo$_2$O$_4$ core/shell structure electrode possesses the high specific capacitance and the good rate capability. This is attributed to the unique 3D array struc-ture, which can reduce the diffusion resistance of protons and enhance ion transport during the charge–discharge process at high current densities. Furthermore, such a vertically aligned CNT/NiCo$_2$O$_4$ core/shell structure electrode has much better rate performance compared with the reported NiCo$_2$O$_4$-based electrode materials, including porous hexagonal NiCo$_2$O$_4$
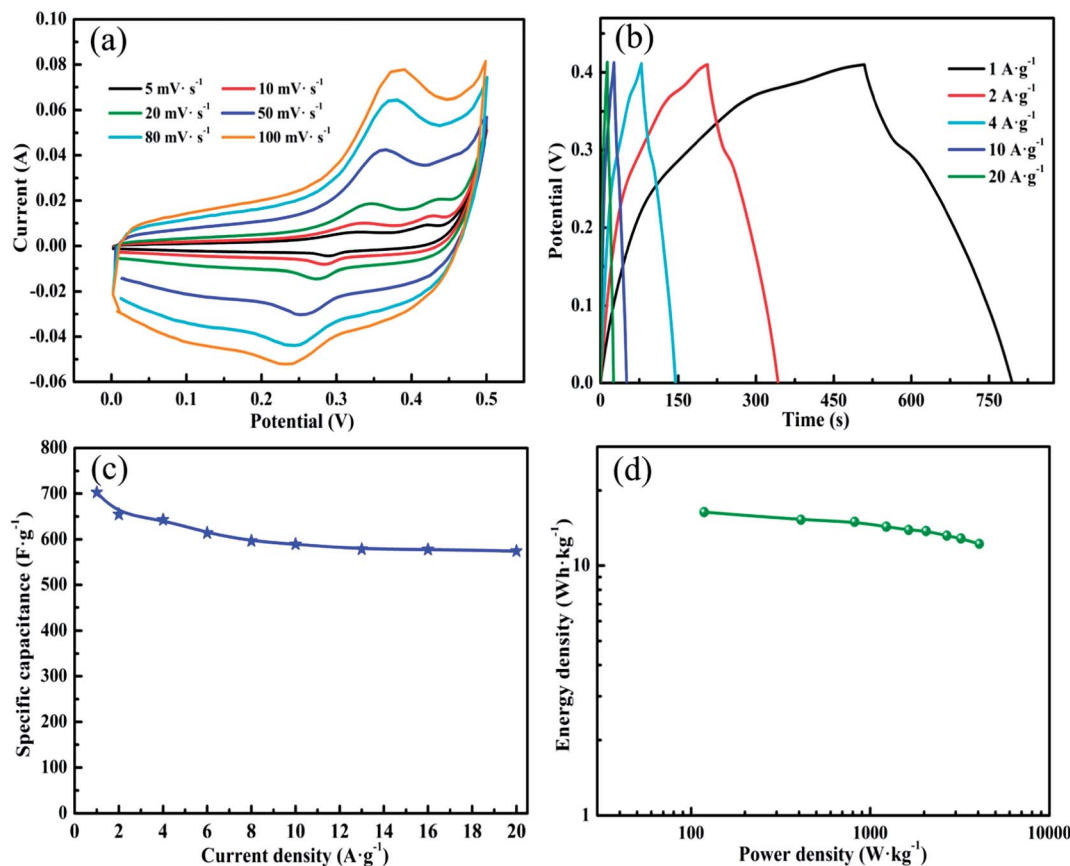
Fig. 5 (a) CV curves at various scan rates, (b) charge/discharge curves at various current densities, (c) calculated specific capacitance as a function of current density, and (d) Ragone plots of the vertically aligned CNT/NiCo$_2$O$_4$ core/shell structure electrode in 6 M KOH electrolyte.

nanoplates, nickel–cobalt nanosheets, hollow NiCo$_2$O$_4$ sub-microspheres, nanostructured NiCo$_2$O$_4$ spinel thin-film electrode, NiCo$_2$O$_4$ nanowire-loaded graphene, NiCo$_2$O$_4$–reduced graphene oxide composite, nickel cobalt oxide–single wall carbon nanotube composite, cobalt nickel oxysulfide (CoNi)O$_x$S$_y$ and so on (the corresponding results are listed in Table 1).[32,39,41,44–53]

Energy density and power density are two key factors to evaluate the applications of supercapacitors. A good electrode material is expected to provide high energy density and high capacitance simultaneously at high charge/discharge rates. Therefore, Ragone plots, the relationship between the energy densities and the power densities calculated from the charge/discharge profiles according to eqn (2) and (3), respectively, are presented in Fig. 4d. It can be observed that, with increased power density, the energy density reduces slowly, which reaches 16.4 W h kg^{-1} at a power density of 118.4 W kg^{-1}, and still remains 13.4 W h kg^{-1} at a power density of 4086.3 W kg^{-1}. These values are comparable with those of the reported NiCo$_2$O$_4$-based electrode materials,[41,44,45,47,49,53] supporting the applicability of the vertically aligned CNT/NiCo$_2$O$_4$ core/shell structures as the very promising electrode material in supercapacitors.

It is well-known that cycle stability is another parameter of great importance to evaluate the performance of

supercapacitors. Thus, the cycle stability of the vertically aligned CNT/NiCo$_2$O$_4$ core/shell structure electrode is examined by the repeated galvanostatic charge/discharge cycle at a current density of 4 A g^{-1}. As shown in Fig. 6, it is noted that the specific capacitance is almost constant with only minor fluctuations during the long cycle process. Importantly, only 9% of the original capacitance is lost after 1500 cycles, indicating that this vertically aligned CNT/NiCo$_2$O$_4$ core/shell structure electrode has good long-term cycle stability. This is also proved by the SEM image of the electrode after long cycling (see ESI Fig. S7†). Clearly, as can be seen in the SEM image, the morphology and structure of the vertically aligned CNT/NiCo$_2$O$_4$ core/shell structure are well retained after 1500 charge/discharge cycles, which strongly demonstrate the good charge/discharge stability and long-term cycle life.

Based on the above electrochemical results, the excellent supercapacitive performances of the vertically aligned CNT/NiCo$_2$O$_4$ core/shell structure electrode, including high specific capacitance, good rate capability and excellent cycle stability, might be attributed to its unique 3D array structure in the following aspects. First, the 3D vertically aligned CNTs "cores" provide a strong skeleton for the NiCo$_2$O$_4$ nanosheets, avoiding their aggregation, retaining the inter-space inside and also the large surface area. Second, the "shell" NiCo$_2$O$_4$ nanosheets with the ultrathin and nanoporous characteristics possess numerous

Table 1 Comparison of the electrochemical performances of the as-prepared CNT/NiCo$_2$O$_4$ composite array with the reported ones

| Material	Preparation method	Specific capacitance (F g^{-1})	Rate performance	Capacity retention	Reference
NiCo$_2$O$_4$ nanoplates	Hydrothermal and calcination	294 (1 A g^{-1})	48% (10 A g^{-1})	89.8% (2200 cycles)	32
Nickel–cobalt nanosheets	Electrochemical deposition	506 (1 A g^{-1})	40% (10 A g^{-1})	94% (2000 cycles)	39
NiCo$_2$O$_4$–RGO	Self-assembly and thermal treatment	835 (1 A g^{-1})	74% (16 A g^{-1})	108% (4000 cycles)	41
NiCo$_2$O$_4$	Self-assembly and thermal treatment	662 (1 A g^{-1})	53% (16 A g^{-1})	52% (4000 cycles)	41
NiCo$_2$O$_4$ sub-microspheres	Template-engaged synthesis	678 (1 A g^{-1})	80% (20 A g^{-1})	87% (3500 cycles)	44
NiCo$_2$O$_4$ thin-film	Electrochemically synthesized	575 (1 A g^{-1})	98% (10 A g^{-1})	99% (1000 cycles)	45
NiCo$_2$O$_4$@RGO	Hydrothermal	737 (1 A g^{-1})	50% (10 A g^{-1})	94% (3000 cycles)	46
NiCo$_2$O$_4$ framework	Polymer-assisted chemical method	587 (2 A g^{-1})	88% (16 A g^{-1})	89% (3500 cycles)	47
(CoNi)O$_x$S$_y$	Hydrothermal	592 (2 A g^{-1})	25% (20 A g^{-1})	95% (2000 cycles)	48
NiCo$_2$O$_4$@NiCo$_2$O$_4$ core/shell	Hydrothermal and chemical deposition	900 (1 A g^{-1})	75% (20 A g^{-1})	98.6% (4000 cycles)	49
NiCo$_2$O$_4$	Hydrothermal	660 (1 A g^{-1})	71% (20 A g^{-1})	66.3% (4000 cycles)	49
NiCo$_2$O$_4$ nanoflakes	Chemical bath deposition	490 (15 A g^{-1})	No data	97% (900 cycles)	50
NiCo$_2$O$_4$ nanorods	Chemical bath deposition	330 (15 A g^{-1})	No data	96% (900 cycles)	50
NiCo$_2$O$_4$ hexagonal	Hydrothermal and annealing	663 (1 A g^{-1})	88% (8 A g^{-1})	88.4% (5000 cycles)	51
Nickel–cobalt hydroxide	Chemical bath deposition	456 (20 mV s^{-1})	70% (200 mV s^{-1})	91% (1000 cycles)	52
NiCo$_2$O$_4$	Sol–gel approach	222 (1 A g^{-1})	84% (3.5 A g^{-1})	96.3% (600 cycles)	53
CNT/NiCo$_2$O$_4$ core/shell	Electrochemical deposition	694 (1 A g^{-1})	82% (20 A g^{-1})	91% (1500 cycles)	This work
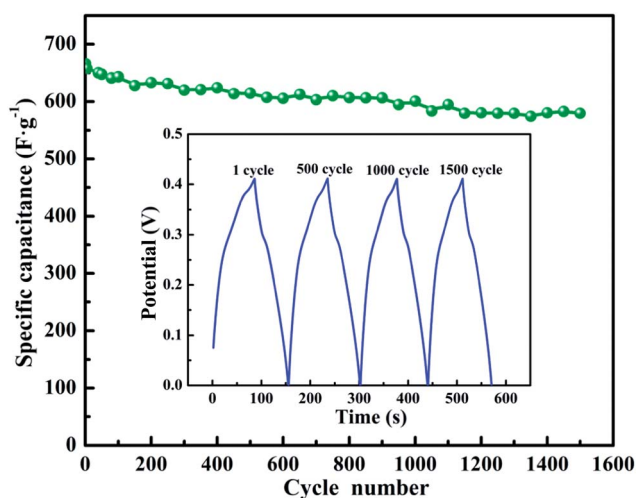
Fig. 6 Variation of the specific capacitance of the vertically aligned CNT/NiCo$_2$O$_4$ core/shell structure electrode as a function of cycle number measured at the current density of 4 A g^{-1} in 6 M KOH electrolyte. The inset image shows the charge/discharge curves of the 1, 500, 1000 and 1500 cycles.

active sites for the redox reaction, ensuring efficient contact between the surface of NiCo$_2$O$_4$ nanosheets and the electrolyte even at high rates, shortening the diffusion pathway and enabling fast ion transport. Third, the open space between the vertically aligned CNT/NiCo$_2$O$_4$ core/shell structures can serve as the ion-buffering reservoirs to minimize the diffusion distance to the interior surfaces, which may accelerate the kinetic process of the ion diffusion in the electrode, hence favoring the high power performance. In addition, highly conductive vertically aligned CNTs directly grown on the SS current collector not only benefits the fast electron transfer but also avoids the use of a polymer binder or conductive additive which commonly adds in extra contact resistance. Because of these intriguing advantages, the excellent electrochemical

performances have been achieved in the vertically aligned CNT/NiCo$_2$O$_4$ core/shell structure electrode.

4. Conclusions

In summary, we have successfully prepared the 3D vertically aligned CNT/NiCo$_2$O$_4$ core/shell structure electrode *via* a facile electrochemical deposition method and subsequent annealing in air. The as-prepared vertically aligned CNT/NiCo$_2$O$_4$ core/shell structure electrode exhibits an initial specific capacitance of 695 F g^{-1} at the current densities of 1 A g^{-1} and 576 F g^{-1} at 20 A g^{-1}. Furthermore, the specific capacitance of the vertically aligned CNT/NiCo$_2$O$_4$ core/shell structure electrode remains 91% of its original capacity at the current density of 4 A g^{-1} after 1500 cycles. The high specific capacitance, remarkable rate capability and excellent cycling ability of the composites are attributed to the unique properties of the 3D vertically aligned CNT/NiCo$_2$O$_4$ core/shell structure, which provide numerous electroactive sites for redox reaction, ensure efficient contact between the surface of NiCo$_2$O$_4$ nanosheets and the electrolyte even at high rates, shorten the diffusion pathway and enable fast ion transport. Predictably, the current study probably gives a new insight for designing and synthesizing 3D core/shell structure electrode materials for high-performance super-capacitors and other energy-storage devices.

References

1 P. Simon and Y. Gogotsi, *Nat. Mater.*, 2008, 7, 845.

5106 | *J. Mater. Chem. A*, 2014, **2**, 5100–5107

This journal is © The Royal Society of Chemistry 2014

2 L. Huang, D. C. Chen, Y. Ding, S. Feng, Z. L. Wang and M. L. Liu, *Nano Lett.*, 2013, **13**, 3135–3139.

3 X. D. Wang, J. H. Song, J. Liu and Z. L. Wang, *Science*, 2007, **316**, 102.

4 W. L. Yang, Z. Gao, J. Ma, X. M. Zhang, J. Wang and J. Y. Liu, *J. Mater. Chem. A*, 2014, **2**, 1448–1457.

5 D. Guo, P. Zhang, H. M. Zhang, X. Z. Yu, J. Zhu, Q. H. Li and T. H. Wang, *J. Mater. Chem. A*, 2013, **1**, 9024.

6 C. Q. Shang, S. M. Dong, S. Wang, D. D. Xiao, P. X. Han, X. G. Wang, L. Gu and G. L. Cui, *ACS Nano*, 2013, **7**, 5430.

7 C.-T. Hsu and C.-C. Hu, *J. Power Sources*, 2013, **242**, 662.

8 F. X. Wang, S. Y. Xiao, Y. Y. Hou, C. L. Hu, L. L. Liu and Y. P. Wu, *RSC Adv.*, 2013, **3**, 13059.

9 A. Ghosh, V. T. Le, J. J. Bae and Y. H. Lee, *Sci. Rep.*, 2013, DOI: 10.1038/srep02939.

10 S. L. Chou, J. Z. Wang, S. Y. Chew, H. K. Liu and S. X. Dou, *Electrochem. Commun.*, 2008, **10**, 1724.

11 M. Kim, Y. Hwang, K. Min and J. Kim, *Phys. Chem. Chem. Phys.*, 2013, **15**, 15602.

12 J. B. Mu, B. Chen, Z. C. Guo, M. Y. Zhang, Z. Y. Zhang, P. Zhang, C. L. Shao and Y. C. Liu, *Nanoscale*, 2011, **3**, 5034.

13 T. Y. Wei, C. H. Chen, K. H. Chang, S. Y. Lu and C. C. Hu, *Chem. Mater.*, 2009, **21**, 3228.

14 B. Wang, T. Zhu, H. B. Wu, R. Xu, J. S. Chen and X. W. Lou, *Nanoscale*, 2012, **4**, 2145.

15 X. X. Qing, S. Q. Liu, K. L. Huang, K. Z. Lv, Y. P. Yang, Z. G. Lu, D. Fang and X. X. Liang, *Electrochim. Acta*, 2011, **56**, 4985.

16 B. Wang, J. S. Chen, Z. Y. Wang, S. Madhavi and X. W. Lou, *Adv. Energy Mater.*, 2012, **2**, 1188.

17 H. W. Park, B.-K. Na, B. W. Cho, S.-M. Parka and K. C. Roh, *Phys. Chem. Chem. Phys.*, 2013, **15**, 17626.

18 P. H. Yang, X. Xiao, Y. Z. Li, Y. Ding, P. F. Qiang, X. H. Tan, W. J. Mai, Z. Y. Lin, W. Z. Wu, T. Q. Li, H. Y. Jin, P. Y. Liu, J. Zhou, C. P. Wong and Z. L. Wang, *ACS Nano*, 2013, **7**, 2617.

19 R. K. Selvan, I. Perelshtein, N. Perkas and A. Gedanken, *J. Phys. Chem. C*, 2008, **112**, 1825.

20 B. Saravanakumar, K. K. Purushothaman and G. Muralidharan, *ACS Appl. Mater. Interfaces*, 2012, **4**, 4484.

21 E. Khoo, J. M. Wang, J. Ma and P. S. Lee, *J. Mater. Chem.*, 2010, **20**, 8368.

22 Q. Li, Z.-L. Wang, G.-R. Li, R. Guo, L.-X. Ding and Y.-X. Tong, *Nano Lett.*, 2012, **12**, 3803.

23 O. Ghodbane, F. Ataherian, N. L. Wu and F. Favier, *J. Power Sources*, 2012, **206**, 454.

24 D. Guo, P. Zhang, H. M. Zhang, X. Z. Yu, J. Zhu, Q. H. Li and T. H. Wang, *J. Mater. Chem. A*, 2013, **1**, 9024.

25 L. Yu, G. Q. Zhang, C. Z. Yuan and X. W. Lou, *Chem. Commun.*, 2013, **49**, 137.

26 H. Jiang, J. Ma and C. Z. Li, *Chem. Commun.*, 2012, **48**, 4465.

27 B. Cui, H. Lin, J. B. Li, X. Li, J. Yang and J. Tao, *Adv. Funct. Mater.*, 2008, **18**, 1440.

28 D. Carriazo, J. Patino, M. C. Gutierrez, M. L. Ferrer and F. D. Monte, *RSC Adv.*, 2013, **3**, 13690.

29 T. Y. Wei, C. H. Chen, H. C. Chien, S. Y. Lu and C. C. Hu, *Adv. Mater.*, 2010, **22**, 347.

30 J. Liu, C. P. Liu, Y. L. Wan, W. Liu, Z. S. Ma, S. M. Ji, J. B. Wang, Y. C. Zhou, P. Hodgson and Y. C. Li, *CrystEngComm*, 2013, **15**, 1578.

31 R. J. Zou, K. B. Xu, T. Wang, G. J. He, Q. Liu, X. J. Liu, Z. Y. Zhang and J. Q. Hu, *J. Mater. Chem. A*, 2013, **1**, 8560.

32 J. Pu, J. Wang, X. Q. Jin, F. Cui, E. H. Sheng and Z. H. Wang, *Electrochim. Acta*, 2013, **106**, 226.

33 G. Q. Zhang, H. B. Wu, H. E. Hoster, M. B. Chan-Park and X. W. Lou, *Energy Environ. Sci.*, 2012, **5**, 9453.

34 L. Yu, H. B. Wu, T. Wu and C. Z. Yuan, *RSC Adv.*, 2013, **3**, 23709.

35 M.-C. Liu, L.-B. Kong, C. Lu, X.-M. Li, Y.-C. Luo and L. Kang, *ACS Appl. Mater. Interfaces*, 2012, **4**, 4631.

36 D. U. Lee, B. J. Kim and Z. W. Chen, *J. Mater. Chem. A*, 2013, **1**, 4754.

37 C. Z. Yuan, J. Y. Li, L. R. Hou, L. Yang, L. F. Shen and X. G. Zhang, *J. Mater. Chem.*, 2012, **22**, 16084.

38 C. Z. Yuan, J. Y. Li, L. R. Hou, X. G. Zhang, L. F. Shen and X. W. Lou, *Adv. Funct. Mater.*, 2012, **22**, 4592.

39 X. H. Lu, X. Huang, S. L. Xie, T. Zhai, C. S. Wang, P. Zhang, M. H. Yu, W. Li, C. L. Liang and Y. X. Tong, *J. Mater. Chem.*, 2012, **22**, 13357.

40 L. Qian, L. Gu, L. Yang, H. Y. Yuan and D. Xiao, *Nanoscale*, 2013, **5**, 7388.

41 H.-W. Wang, Z.-A. Hu, Y.-Q. Chang, Y.-L. Chen, H.-Y. Wu, Z.-Y. Zhang and Y.-Y. Yang, *J. Mater. Chem.*, 2011, **21**, 10504.

42 Y. J. Kang, H. Chung, C.-H. Han and W. Kim, *Nanotechnology*, 2012, **23**, 065401.

43 X. Y. Liu, Y. Q. Zhang, X. H. Xia, S. J. Shi, Y. Lu, X. L. Wang, C. D. Gu and J. P. Tu, *J. Power Sources*, 2013, **239**, 157.

44 C. Z. Yuan, J. Y. Li, L. R. Hou, J. D. Lin, G. Pang, L. H. Zhang, L. Lian and X. G. Zhang, *RSC Adv.*, 2013, **3**, 18573.

45 V. Gupta, S. Gupta and N. Miura, *J. Power Sources*, 2010, **195**, 3757.

46 G. Y. He, L. Wang, H. Q. Chen, X. Q. Sun and X. Wang, *Mater. Lett.*, 2013, **98**, 164.

47 C. Z. Yuan, J. Y. Li, L. R. Hou, J. D. Lin, X. G. Zhang and S. L. Xiong, *J. Mater. Chem. A*, 2013, **1**, 11145.

48 L. F. Liu, *Nanoscale*, 2013, **5**, 11615.

49 X. Y. Liu, S. J. Shi, Q. Q. Xiong, L. Li, Y. J. Zhang, H. Tang, C. D. Gu, X. L. Wang and J. P. Tu, *ACS Appl. Mater. Interfaces*, 2013, **5**, 8790.

50 R. R. Salunkhe, K. Jang, H. Yu, S. Yu, T. Ganesh, S.-H. Han and H. Ahn, *J. Alloys Compd.*, 2011, **509**, 6677.

51 J. Pu, X. Q. Jin, J. Wang, F. L. Cui, S. B. Chu, E. H. Sheng and Z. H. Wang, *J. Electroanal. Chem.*, 2013, **707**, 66.

52 R. R. Salunkhe, K. Jang, S.-W. Lee and H. Ahn, *RSC Adv.*, 2012, **2**, 3190.

53 Y. Q. Wu, X. Y. Chen, P. T. Ji and Q. Q. Zhou, *Electrochim. Acta*, 2011, **56**, 7517.

This journal is © The Royal Society of Chemistry 2014

J. Mater. Chem. A, 2014, **2**, 5100–5107 | **5107**